

## Two-qubit gate based on a multiterminal double-barrier Josephson junction

S. E. Shafranjuk\*

*Department of Physics and Astronomy, Northwestern University, Evanston, Illinois 60208, USA*

(Received 17 January 2006; revised manuscript received 1 May 2006; published 26 July 2006)

A multiterminal double-barrier SISIS junction (S and I denote a superconductor and an insulating barrier, respectively) is suggested as a two-qubit gate with tunable intrinsic coupling. Two quantum wells are formed in the vicinities of the left and right SIS subjunctions. This gives two individual qubits, which are intrinsically coupled via the middle S layer due to phase coherence. The interqubit coupling  $J$  is tuned by two bias supercurrents  $I_1$  and  $I_2$  across each of the SIS subjunctions independently. Additional coupling is accomplished by transport supercurrents  $I_1^{\text{tr}}$  along adjacent S layers. Using a microscopic model we compute major qubit characteristics and study sources of the intrinsic decoherence. We compute the entanglement of the two-qubit states, leakage and fidelity characteristics versus  $J$ , and discuss the readout process.

DOI: [10.1103/PhysRevB.74.024521](https://doi.org/10.1103/PhysRevB.74.024521)

PACS number(s): 74.50.+r, 73.40.Gk, 03.65.-w, 03.67.Mn

### I. INTRODUCTION

Interest in Josephson junction-based two-qubit gates,<sup>1,2</sup> which serve as building blocks for quantum computers, was inspired by experimental demonstrations of single qubits.<sup>3-9</sup> Each qubit is a two-state quantum system, which behaves like a spin-1/2 particle and can be entangled with other qubits. In recent experiments,<sup>1,2</sup> a quantum-coherent dynamics of two Josephson qubits coupled through a capacitance was studied. A tunable interaction between different types of Josephson qubits was examined also theoretically (see Refs. 10-12 and the references therein). The qubit gate<sup>10-12</sup> consisted of two current-biased Josephson junctions coupled via a capacitance, which allowed the performance of arbitrary two-qubit quantum logic operations.

The method of capacitive coupling has, however, certain disadvantages. In particular, additional circuit elements and wiring serve as potential sources of disturbance in the system: the electric charges, accumulated on the capacitance, disturb the quantum states and cause errors during quantum logic operations. An alternative way to introduce a tunable coupling between different quantum subsystems is to exploit a bias-tuned intrinsic coupling taking place in multilayered multiterminal structures.<sup>13,14</sup> Though general properties of the intrinsic entanglement in a solid-state device were considered earlier (see, e.g., Ref. 15 and references therein), its implementation to two-qubit gates is not well known yet.

In this work we study a simple two-qubit gate based upon the intrinsic properties of a double-barrier multiterminal SISIS junction (S is the superconductor; I is the insulating barrier) with a proximity-type coupling between the left and right SIS subjunctions (see Fig. 1) across their common S layer. Elementary quantum logic operations on qubits<sup>3-9</sup> are associated with controlled manipulations involving two states  $|0\rangle$  and  $|1\rangle$  of the same qubit, the superposition of which forms a mixed state  $|\Psi\rangle$ . Quantum computing presumes also the superposition  $|\Phi_{1,2}\rangle$  of the states  $|\alpha_1\rangle$  and  $|\beta_2\rangle$  of two different qubits 1 and 2. An ideal two-qubit Hamiltonian in spin-1/2 notation takes the form<sup>16</sup>

$$\hat{H}_q = \sum_{k=1,2} [\varepsilon^{(k)} \hat{\sigma}_z^k + \tau^{(k)} \hat{\sigma}_x^k + \hat{\alpha}_k] + \sum_{nm} J_{nm} (i\hat{\sigma}_n^1) \otimes (i\hat{\sigma}_m^2), \quad (1)$$

where  $\varepsilon^{(k)}$  and  $\tau^{(k)}$  are the energy level spacing and the interlevel tunneling matrix element in the  $k$ th qubit,  $\hat{\sigma}_n^1$  and  $\hat{\sigma}_m^2$  are Pauli matrices associated with the first and second qubits;  $J_{nm}$  is the interqubit coupling energy,  $\{n, m\} = \{x, y, z\}$ . Each of the qubits is independently controlled by fields  $\hat{\alpha}_k = \alpha_k \exp[i\hat{\sigma}_y^k \theta_k(t)]$ , where  $\alpha_k$  and  $\theta_k$  are control field amplitudes and phases, and  $k=1, 2$ . For controlled manipulations of the qubit the coefficients of the Hamiltonian are modified by an adiabatic change of the Josephson supercurrents. The adiabaticity is required to eliminate transitions between different two-qubit gate states. The parameters of Eq. (1) depend also on the particular design of the qubit gate and will be discussed in more detail in Sec. IV. Each of the qubits in the two-qubit gate described by Eq. (1) should behave indi-

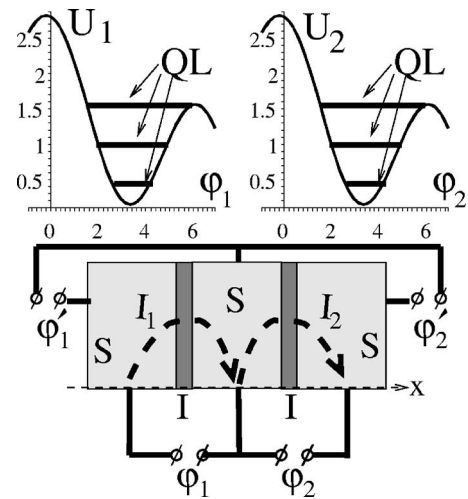


FIG. 1. The quantized levels (QL's) formed inside the quantum wells  $U_1$  and  $U_2$  controlled by bias supercurrent  $I_1$  and  $I_2$  across the SIS subjunctions of a multiterminal SISIS junction. The phase differences  $\varphi'_1 \neq \varphi_1$  and  $\varphi'_2 \neq \varphi_2$  if transport supercurrents  $I_1^{\text{tr}}$  flow along the S electrodes.

vidually. One assumes that ac control pulses address both qubits with no disturbance of other circuit elements. The two qubits labeled as 1 and 2 are built using the tilted washboard Josephson energy potentials  $U_1(\varphi_1)$  and  $U_2(\varphi_2)$  where  $\varphi_1$  and  $\varphi_2$  are the phase differences across the left (1) and right (2) SIS subjunctions. The sets of quantized energy levels (QL's) positioned at  $\varepsilon_n^{(l)}$  ( $l$  is the qubit index and  $n$  is the level quantum number) are formed in the washboard quantum wells  $U_1$  and  $U_2$ . The tilting of  $U_1$  and  $U_2$  is controlled by the bias supercurrents  $I_1$  and  $I_2$  as shown in the lower part of Fig. 1. We will see that the directions and magnitudes of  $I_1$  and  $I_2$  not only affect the interlevel spacing  $\varepsilon^l = \varepsilon_1^l - \varepsilon_0^l$  ( $l = 1, 2$ ) in both qubits but actually determine the strength of the interqubit interaction  $J_{nm}$ . In this way one accomplishes arbitrary single- and two-qubit quantum logic operations by applying appropriate ac and dc bias currents to the SIS subjunctions.

The paper is organized as follows. In next section II we compute the proximity coupling between two SIS subjunctions across their common interstitial S layer versus partial phase differences  $\varphi_1$  and  $\varphi_2$ . In Sec. III we compute the interqubit coupling energy  $J_{\max}$  versus the middle S layer thickness  $d$  and the elastic electron mean free path  $l_i$ . In Sec. IV we determine how the interqubit coupling is controlled by the bias supercurrents  $I_1$  and  $I_2$  across the SIS subjunctions. We also will discuss parameters of the two-qubit gate Hamiltonian (1) for our setup. In Sec. V we analyze an additional control over the two-qubit gate accomplished when applying transport supercurrents  $I_i^r$  along adjacent layers in each subjunction. In Sec. VI we study the intrinsic source of errors in our two-qubit gate and calculate the leakage and fidelity. We also discuss the dissipation introduced by the readout process.

## II. PROXIMITY COUPLING IN A MULTILAYERED JUNCTION

The coupling between the left and right SIS subjunctions of the SISIS junction [see Figs. 1 and 2(a)] is conveniently described in terms of Andreev reflection. Here we are interested in a nonlocal process when an incoming electron and the reflected hole belong to different electrodes spatially separated by a distance  $\sim \xi$ , where  $\xi$  is the superconducting coherence length (see, e.g., Ref. 13 and references therein). Though the two electrodes are separated, they couple via the superfluid condensate. Following Refs. 13 and 18 we quote this process as a nonlocal Andreev (NA) reflection. The NA process is actually equivalent to injecting of two spin-entangled electrons, which form a singlet state of a Cooper pair spread between two different leads.<sup>18</sup> The NA was studied experimentally in Ref. 13 using a double-barrier three-terminal NISIN junction (N is the normal metal). Similar double-barrier three-terminal SINIS devices were recently examined also in Ref. 19. The quantized oscillation spectrum of a highly transparent SISIS junction was studied in Ref. 14. The coherent interaction through the double-barrier junction is noticeable even if the barrier transparency is relatively low (i.e.,  $D \approx 10^{-5}$ , as in the NISIN structures used in Ref. 13). Then, the quantum coherence (QC) established across the

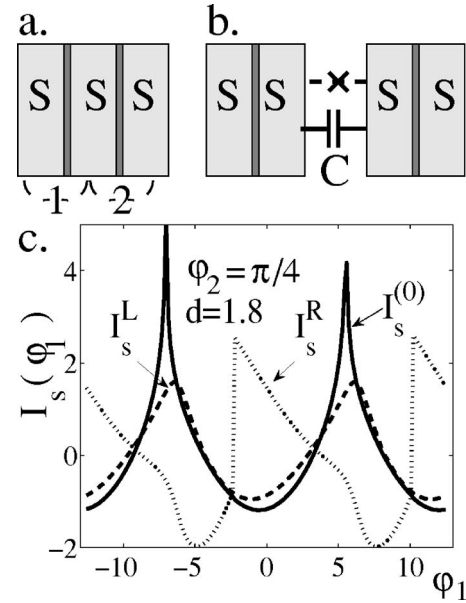


FIG. 2. (a) The two subjunctions of the SISIS junction. (b) Two SIS junctions coupled capacitively. The dashed line with a cross indicates that the coupling is not phase coherent. (c) The current-phase relationship in the two-barrier multiterminal junction.

whole SISIS junction yields a finite coupling between the right and left SIS subjunctions via their common middle S layer.

The QC coupling energy  $J_{12}$  between the two subjunctions 1 and 2 [see Fig. 2(a)] is defined as<sup>20</sup>

$$J_{12}(\varphi_2) = \max_{\varphi_1} \{W - W^{(0)}\}, \quad (2)$$

where  $W(\varphi) = \int \varphi I_s^{\text{SISIS}}(\varphi') d\varphi'$  is the energy of the whole SISIS junction. The energy of two single SIS junctions connected in series [see Fig. 2(b)] is  $W^{(0)}(\varphi) = 2 \int \varphi I_s^{\text{SIS}}(\varphi') d\varphi'$ . The two energies  $W$  and  $W^{(0)}$  are not equal to each other because the current across the middle electrode of SISIS junction is evidently a phase-coherent supercurrent, while the electric current between two single SIS junctions connected in a sequence [as shown by the dashed line with a cross in Fig. 2(b)] is not phase coherent. This difference between  $W$  and  $W^{(0)}$  coming from the phase coherence in SISIS serves as a source of our intersubjunction coupling. The QC coupling between the left and right SIS subjunctions may be tuned by attaching a third terminal to their common S layer. Then the phase differences  $\varphi_1$  and  $\varphi_2$  across the left and right barriers of the SISIS junction are controlled independently from each other and the quantum states of each subjunction are addressed individually. Though a microscopic calculation of  $J$  may be performed in various ways, here we implement a quasiclassical Green function method with special boundary conditions at the interface barriers.<sup>20-24</sup> The approach<sup>20-24</sup> allows a direct microscopic delineation of the interjunction coupling and is applicable to junctions with arbitrary interface transparency and purity of the electrodes.

The QC coupling is tuned by the bias supercurrents  $I_1$  and  $I_2$ . The bias is applied to each of the SIS subjunctions individually, as shown in Fig. 1. If  $I_1 \neq I_2$ , then the corresponding phase differences  $\varphi_1$  and  $\varphi_2$  are not equal to each other (i.e.,  $\varphi_1 \neq \varphi_2$ ), while the net supercurrent  $I_s(\varphi_1, \varphi_2, x)$  inside the middle S layer of the SIS junction depends also on the coordinate  $x$  in the direction perpendicular to interfaces.

The approach<sup>20–24</sup> gives a tractable microscopic description of the bias-controlled QC effect in multilayered superconducting junctions. The basic elementary process responsible for the coherent coupling in the system is the Andreev reflection. In the terms of Refs. 21–24, a moving hole creates a new electron with a reversed trajectory of motion. Most important is that the multiple processes of the electron-hole conversion keep the packet on a classical trajectory in the  $\mathbf{r}$ - $\mathbf{p}$  space. The particles may switch to another classical trajectory at the knots, where the scattering occurs with a certain probability described by special boundary conditions.<sup>22,23</sup> The quasiclassical approximation had proven to be effective when studying phase-coherent transport in multilayered superconducting structures.<sup>14,24</sup> The nonuniform supercurrent  $I_s(\varphi_1, \varphi_2, x)$  is obtained from the one-point quasiclassical Green function  $\hat{g}$  as

$$I_s(\varphi_1, \varphi_2, x) = \frac{\pi e \hbar p_F}{2m} \nu_0 \int d\varepsilon \int_{-1}^1 \eta d\eta \text{Tr}\{\text{Im} \hat{g}(\varepsilon, \eta, \varphi_1, \varphi_2, x)\}, \quad (3)$$

where  $\eta = \cos \vartheta$ ,  $\vartheta$  being the electron incidence angle,  $p_F$  is the Fermi momentum, and  $\nu_0$  is the normal electron density of states at the Fermi level. The Green function  $\hat{g}$  in Eq. (3) is expressed as

$$\hat{g}(x) = [\bar{\psi}_-(x) \psi_+(x)]^{-1} [\psi_+(x) \bar{\psi}_-(x) + \psi_-(x) \bar{\psi}_+(x)], \quad (4)$$

where spinors  $\psi_{\pm}(x)$  are  $\bar{\psi} = -i\psi^T \hat{\sigma}_y = (v-u)$  and  $\mathcal{T}$  means transposing. The electron and hole envelope wave functions  $u$  and  $v$  are defined on classical trajectories. The trajectories are coupled to each other at the knots, associated with the interface barriers. The nonuniform supercurrent (3) is used to control the coupling between the two SIS subjunctions as will be discussed in the next section.

### III. INTERQUBIT COUPLING ENERGY

The interqubit coupling energy  $J_{12}$  is computed using Eqs. (3) and (4). The microscopic equations (3) and (4) describe the properties of junctions with arbitrary transparency. They allow accounting for the tunneling across the interface barriers  $I$ , for the elastic electron scattering on atomic impurities, and for the inelastic scattering on phonons in the junction's electrodes. As a first step toward computing  $J_{12}$  we solve the quasiclassical Andreev equation  $\hat{H}\psi = E\psi$  for  $\psi_+(x)$  and  $\psi_-(x)$ . The equation is completed by special boundary conditions<sup>22–24</sup> at the interface barrier positions  $x = x_{L(R)}$  and at  $x = \pm\infty$  for the geometry of Fig. 1. The solution serves as a plug into Eq. (4) for the quasiclassical retarded Green function  $\hat{g}(x)$ . Substituting  $\hat{g}(x)$  into Eq. (3) one computes the total supercurrent  $I_s(\varphi_1, \varphi_2, x)$ . The local current-phase rela-

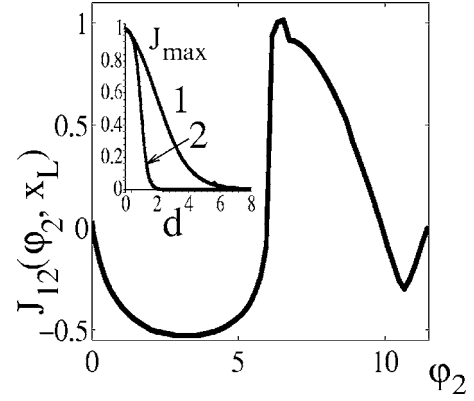


FIG. 3. The QC coupling energy of the left SIS subjunction. The inset shows the maximum coupling strength  $J_{max}$  versus the thickness of the middle layer for “clean” (curve 1) and “dirty” limits (curve 2).

tionships obtained for  $I_s$  inside the middle layer of the SIS junction are shown in Fig. 2(c) where  $I_s$  is denoted as  $I_s^L(\varphi_1)$  for fixed  $\varphi_2 = \pi/4$  at the left barrier  $x = x_L$ , as  $I_s^{(0)}(\varphi_1)$  at the middle of the junction  $x = 0$ , and as  $I_s^R(\varphi_1)$  at the right barrier  $x = x_R$ . Here we assume that  $\varphi'_{1,2} = \varphi_{1,2}$ . Then the local supercurrent  $I_s(x)$  depends upon two phase differences  $\varphi_1$  and  $\varphi_2$ ; therefore, one may define a critical supercurrent with respect just to one variable (e.g.,  $\varphi_1$ ) and consider its dependence versus another variable (i.e.,  $\varphi_2$ ). This behavior is interpreted as the QC coupling between the two SIS subjunctions of a symmetric SIS junction characterized by an energy  $J(\varphi_1, \varphi_2)$ . The coupling energy of the left SIS subjunction, which depends also on the phase difference across the right SIS subjunction  $\varphi_2$ , is obtained from Eq. (2). In Eq. (2),

$$W(\varphi_1, \varphi_2) = \frac{\Phi_0}{2\pi} I_c - \frac{1}{2} W_1(\varphi_1, \varphi_2) - \frac{1}{2} W_2(\varphi_1, \varphi_2) \quad (5)$$

is the SIS “washboard” Josephson energy. In Eq. (5),  $I_c$  is the absolute (i.e., with respect to both  $\varphi_1$  and  $\varphi_2$ ) critical current of the SIS junction while the Josephson energy of the coupled SIS subjunction 1(2) is defined as

$$W_{1(2)}(\varphi_1, \varphi_2) = \frac{\Phi_0}{2\pi} \int_{-\infty}^{\varphi_1(2)} I_s(\varphi_1, \varphi_2, x_L) d\varphi_{1(2)}. \quad (6)$$

Equation (2) completed by Eqs. (3)–(6), constitutes the QC coupling  $J_{12}(\varphi_2)$  of the left SIS subjunction to the right SIS subjunction versus  $\varphi_1$  and  $\varphi_2$ , tuned by corresponding bias supercurrents  $I_1$  and  $I_2$  (assuming here that  $\varphi'_1 = \varphi_1$  and  $\varphi'_2 = \varphi_2$ ). We emphasize that the coupling  $J_{12}$  comes entirely from the phase coherence between the two SIS subjunctions.

The computed dependence  $J_{12}(\varphi_2)$  at  $x = x_L$  is plotted in Fig. 3, from which one can see that the sign and magnitude of  $J_{12}(\varphi_2)$  are controlled by the phase difference  $\varphi_2$  across the counterpart SIS subjunction. The QC coupling magnitude  $J(d) = \max_{\varphi_2} \{J_{12}(\varphi_2)\}$  ( $d$  is the middle layer thickness in units of the BCS coherence length) is plotted in the inset to Fig. 3, which shows how  $J$  depends on the thickness and purity of the middle layer characterized by the electron elastic mean free path  $l_i$ : if it is very thick ( $d \gg \xi$ ), the mutual interaction

of subjunctions  $J$  vanishes. When the electron motion inside the middle layer is ballistic ( $l_i \geq \xi$ ), the SIS subjunctions interact with each other though the middle layer is relatively thick (curve 1 in Fig. 3 for which  $l_i = 5\xi$ ). If, however, the middle layer is impure, the coupling range shortens,  $\xi^* \approx \sqrt{\xi} l_i$ , which is confirmed by our numerical calculations of  $J$  (see curve 2 in Fig. 3 computed for  $l_i = 0.3\xi$ ). This circumstance can be utilized to optimize the coupling in two-qubit gates.

#### IV. CONTROL OF THE INTERQUBIT COUPLING

In the setup shown in Fig. 1, the two SIS subjunctions are used as two coherently coupled qubits. The two-qubit idle state  $|\Phi_{1,2}\rangle$  is realized when the strength  $J_{12}$  of the interqubit coupling vanishes at some value of  $\varphi_2$ . The manipulations with quantum states and the interqubit coupling are controlled by applying bias voltages and supercurrents between the S electrodes. An additional independent control is furnished when  $\varphi'_1 \neq \varphi_1$  and  $\varphi'_2 \neq \varphi_2$  (see Fig. 1) as will be discussed in next section. In this section we analyze basic two-qubit gate parameters (i.e., the level splitting  $\varepsilon$  and the interqubit coupling strength  $J$ ) semiquantitatively. We give a simple illustration to our description using approximate formulas. The properties of each individual SIS qubit, either 1 or 2, are conveniently described as the motion of a particle with mass  $C_{1(2)}$  in the “tilted washboard” potential

$$U_{1(2)} = W_{1(2)} - \frac{\Phi_0}{2\pi} I_{1(2)} \varphi_{1(2)}. \quad (7)$$

The motion inside the quantum well leads to quantized states as sketched in the upper part of Fig. 1. The Josephson energy (JE)  $W_{1(2)}$  of an SIS subjunction 1(2) entering Eq. (7) is given by Eq. (6). The subjunction 1(2) is coupled to its counterpart subjunction 2(1). The quantum eigenstates and eigenvalues of the system in the potential  $U_{1(2)}$  are obtained numerically for a given geometry of the double-barrier junction. The input parameters for numeric computations include the capacitances  $C_{1,2}$  of the left (right) SIS subjunctions, the S layer thickness  $d_S$ , the barrier transparency  $D$ , the junction area  $A$ , the energy gap  $\Delta$ , the elastic electron-impurity scattering rate  $\gamma_i$ , and the control supercurrents  $I_{1,2}$ . The interlevel spacing  $\varepsilon^{(l)} = \varepsilon_1^{(l)} - \varepsilon_2^{(l)}$  is tuned by altering  $I_l$ . Typically, one sets the JE profiles to exploit just two levels in each quantum well, while the third level (used for the read-out of the quantum state) is positioned just below the top of the well (see the upper part of Fig. 1), which is achieved in large-area junctions when  $I_c \Phi_0 / 2\pi \gg e^2 / 2C$  and  $I_c - I_{1,2} \ll I_c$ . In this approximation, the SIS junction behaves like a non-relativistic two-body system. Then the whole behavior of the SIS junction is reduced to a trivial motion of the center of mass. The relative one-body motion is executed by a particle of mass  $C = C_1 C_2 / (C_1 + C_2)$  (where  $C_1$  and  $C_2$  are the capacitances of the left and right SIS subjunctions). The motion is described by a “coordinate”  $\phi = \varphi_1 - \varphi_2$  about a fixed center under the action of an “elastic force”  $F_\phi = -\partial U(\phi) / \partial \phi$ . Here we are interested in the relative motion of the reduced “mass”  $C$  in the two-well model potential  $U(\phi)$  shown in

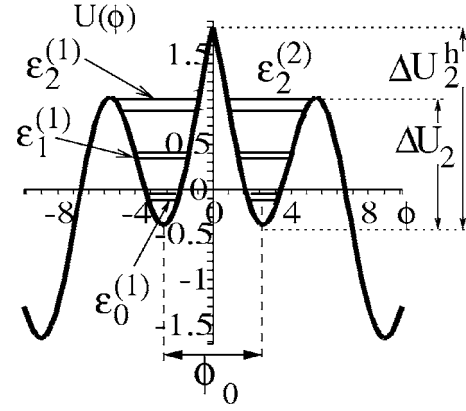


FIG. 4. A two-qubit gate potential with two wells separated by a hump, which is controlled by the bias supercurrents  $I_1$  and  $I_2$ . The quantized levels  $\varepsilon_n^{(l)}$  are formed in each of the wells ( $l=1,2$ ), while the interlevel splitting  $\delta\varepsilon_n^{(l)}$  is controlled by the hump height  $\Delta U_{1,2}^h$  (in general  $\Delta U_1^h \neq \Delta U_2^h$ , if the symmetry is not maintained).

Fig. 4. Simple analytical formulas are obtained when the two-well  $U(\phi)$  is further approximated by a function pieced together from two cubic parabolas. Each of the cubic parabolas has a quadratic curvature at the bottom, which gives a classical oscillation frequency

$$\omega_l \approx 2^{1/4} \sqrt{\frac{2\pi I_l}{\Phi_0 C}} \left(1 - \frac{I_l}{I_c}\right)^{1/4} \quad (8)$$

controlled by the supercurrent  $I_l$ .

The two characteristic barriers in the model potential  $U(\phi)$  have the height

$$\Delta U_l \approx 2\sqrt{2} \frac{I_c \Phi_0}{3\pi} \left(1 - \frac{I_l}{I_c}\right)^{3/2}, \quad (9)$$

where  $l$  is related to the left ( $l=1$ ) and right ( $l=2$ ) wells. The two wells are separated by a hump, which in a symmetric case has the height  $\Delta U^h \approx C\omega_p^2 \phi_0^2 / 2$  where  $\phi_0$  is the distance between the two wells (see Fig. 4). Although the applicability of such an approximation is limited, it serves as a good illustration when modeling qubit switches. Generally speaking, the energy spacing  $\varepsilon^{(l)} = \varepsilon_1^{(l)} - \varepsilon_0^{(l)}$  and the tunneling matrix element  $\tau$ , which enter Hamiltonian (1), depend on the reduced phase difference  $\phi$  in quite a complicated way. A finite interqubit coupling  $J \neq 0$  splits each level additionally—i.e.,  $\varepsilon_n^{(l)} \rightarrow \varepsilon_n^{(l)\pm}$  ( $n=0, \dots, 3$  and  $l=1,2$ )—so the relevant splitting magnitude is  $\delta\varepsilon_n^{(l)} = \varepsilon_n^{(l)+} - \varepsilon_n^{(l)-}$ . In the limit of a weak interqubit coupling, for a symmetric two-qubit gate, within our two-body motion model one approximately finds<sup>27</sup>

$$\delta\varepsilon_n^{(1)} \approx 2\hbar\omega_p(\sigma/2\pi)^{1/2} \exp(-\sigma) \quad (10)$$

and

$$\delta\varepsilon_n^{(2)} \approx 2\hbar\omega_p(\sigma/\pi)^{1/2} \exp(-\sigma), \quad (11)$$

where  $\sigma = C\omega_p \phi_0^2 / \hbar$  and the quantized level energies of a noninteracting qubit are

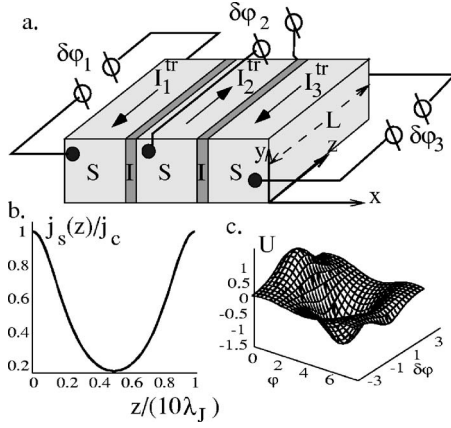


FIG. 5. (a) An additional control of the two-qubit states  $|\Phi_{1,2}\rangle$  with transport supercurrents  $I_p^{\text{tr}}$  flowing in the adjacent S layers. (b) A nonuniform distribution of the supercurrent  $j_s(z)$  versus the lateral coordinate  $z$  (in units of  $10\lambda_J/L$ ) along adjacent S layers. (c) The Josephson energy potential  $U(\varphi, \delta\varphi)$ .

$$\varepsilon_1 \approx \varepsilon_0 + \omega_p [1 - (5/36)(\hbar\omega_p/\Delta U)] \quad (12)$$

and

$$\varepsilon_2 \approx \varepsilon_1 + \omega_p [1 - (11/36)(\hbar\omega_p/\Delta U)]. \quad (13)$$

In the above formulas we omitted the qubit index  $l$  for brevity.

## V. ADDITIONAL CONTROL BY TRANSPORT SUPERCURRENTS

The two-qubit quantum state  $|\Phi_{1,2}\rangle$  is controlled by two bias supercurrents  $I_1$  and  $I_2$  as shown in Fig. 1. By changing the magnitude and direction of both  $I_1$  and  $I_2$  one shifts the quantized level positions  $\varepsilon_n^{(l)}$  and their splitting  $\delta\varepsilon_n^{(l)}$ . However, the two parameters  $I_1$  and  $I_2$  are generally not enough for a full control of the two-qubit gate. In addition to manipulating each individual qubit one must tune the interqubit coupling as well. This requires three independent control parameters at least. An additional independent control over the two-qubit gate is accomplished by applying transport supercurrents  $I_k^{\text{tr}}$  ( $k=1, \dots, 3$ ) along the S electrodes as shown in Fig. 5(a) (see also Fig. 1). If the magnitudes of  $\delta I_1^{\text{tr}} = I_1^{\text{tr}} - I_2^{\text{tr}}$  and  $\delta I_2^{\text{tr}} = I_2^{\text{tr}} - I_3^{\text{tr}}$  are finite, the washboard Josephson energy  $U$  is modified, which in turn changes the two-qubit state  $|\Phi_{1,2}\rangle$ . When the SISIS junction in the lateral  $z$  direction is sufficiently long—i.e.,  $L \gg \lambda_J$  (where  $\lambda_J = \hbar c^2 / [8\pi e(2\lambda_L + d_B)j_c]$  being the Josephson penetration depth,  $\lambda_L$  the London penetration depth,  $d_B$  the thickness of the insulating barrier, and  $j_c$  the Josephson critical supercurrent density)—the distribution of Josephson supercurrent  $j_s(z)$  inside each of the SIS subjunctions becomes nonuniform<sup>28</sup> and depends also on the lateral coordinate  $z$  [see Fig. 5(a)]. Such an inhomogeneous distribution of the supercurrent density  $j_s$  across each of the SIS subjunctions causes a finite phase change  $\delta\varphi_l$  along the  $z$  direction providing that  $\delta\varphi_1 = \varphi'_1 - \varphi_1 \neq 0$  and  $\delta\varphi_2 = \varphi'_2 - \varphi_2 \neq 0$  (see also Fig. 1). This situation resembles the penetration of magnetic flux into a long Josephson junction.<sup>28</sup> In our case

$\delta I_l^{\text{tr}}$  plays a role similar to the  $y$  component of the external dc magnetic field  $\mathcal{H}_y$ , which was the case in Ref. 28. According to Ref. 28, the  $j_s(z)$  profile depends on the ratio  $L/\lambda_J$ : the supercurrent density is highly inhomogeneous for large  $L/\lambda_J$  when a magnetic flux enters the subjunction. An actual  $j_s(z)$  dependence versus  $\delta I_l^{\text{tr}}$  is obtained from the sine-Gordon equation

$$\frac{\partial^2 \varphi_l}{\partial z^2} = \frac{1}{\lambda_J} \sin \varphi_l \quad (14)$$

completed by the boundary conditions  $(\partial\varphi_l/\partial z)|_{z=0}=0$  and  $(\partial\varphi_l/\partial z)|_{z=L} = \delta I_l^{\text{tr}}/en_s = \zeta$ , where  $n_s$  is the superfluid charge carrier concentration.<sup>21</sup> In the BCS approximation one gets  $n_s = \pi n \Delta^2 T \sum_k [\pi^2 T^2 (2k+1)^2 + \Delta^2]^{-3/2}$ , where  $n$  is the normal charge carrier concentration,  $T$  is the temperature, and  $\Delta$  is the energy gap.

The solution  $\varphi_l(z)$  of Eq. (14) is given in elliptic functions.<sup>17</sup> In Fig. 5(b) we show a typical distribution of the supercurrent  $j_s(z)/j_c$  along the left subjunction with  $L/\lambda_J = 10$  and  $\delta I_1^{\text{tr}} = 0$ . In Fig. 5(c) we plot the Josephson energy profile  $U_1(\varphi_1, \delta\varphi_1)$  in the left quantum well at fixed  $I_2$  for a long junction with  $L/\lambda_J = 10$ . One can see that the  $U_l$  profile depends on  $\delta\varphi_l$  (which actually is  $\propto \delta I_l^{\text{tr}}$ ). The transport supercurrents  $I_{1,2}^{\text{tr}}$  renormalize the height of the characteristic barriers  $\Delta U_{1,2}(\phi)$  which acquire the dependence on  $\zeta = \delta I_l^{\text{tr}}/en_s$ . From Eq. (14) at  $z \ll \lambda_J$  and  $\zeta \ll I_c/en_s$  one finds

$$\Delta U_{1,2}(\phi, \zeta) \approx \frac{\Delta U_{1,2}(\phi, \zeta=0)}{Z(\phi, \zeta)}, \quad (15)$$

where  $\Delta U_{1,2}(\phi, \zeta=0) = \Delta U_{1,2}(\phi)$  and the renormalizing function is

$$\frac{1}{Z(\phi, \zeta)} = 1 + \left( \frac{\nu_\phi \zeta}{v_\phi} + \frac{1 - \nu_\phi \zeta^2}{2v_\phi} \right) \left( 1 + \frac{z^2}{2\lambda_J} \right), \quad (16)$$

and we denoted  $\nu_\phi = \Delta U(\phi)/\Delta U_0$ ,  $\Delta U_0 = \Delta U(\phi)|_{\phi=0}$ ,  $\nu_\phi = \partial\nu_\phi/\partial\phi$ . For a noninteracting junction  $\nu_\phi = 1 - \cos\phi$ , while for the subjunctions of the SISIS junction the expression for  $\nu_\phi$  is more complicated and is obtained numerically for a given S layer thickness  $d_S$ , barrier transparency  $D$ , junction area  $A$ , energy gap  $\Delta$ , elastic electron-impurity scattering time  $\tau_i$ , and control supercurrents  $I_{1,2}^{\text{tr}}$ . When finite transport supercurrents  $I_{1,2}^{\text{tr}} \neq 0$  are applied, the levels  $\varepsilon_{1,2}$  are shifted versus  $\zeta$ . The characteristic barriers  $\Delta U_{1,2}$  [see Eq. (9)] entering Eqs. (12) and (13) for  $\varepsilon_{1,2}$  are renormalized by  $Z(\phi, \zeta)$  as follows from Eqs. (15) and (16). In this way, Eqs. (9), (12), and (13) in conjunction with Eqs. (15) and (16) constitute the energy level dispersion versus the control transport supercurrents  $I_{1,2}^{\text{tr}}$ . Our solution demonstrates that the two-qubit states  $|\Phi_{1,2}\rangle$  are readily controlled by the transport supercurrents  $I_{1,2}^{\text{tr}}$  in addition to the bias supercurrents  $I_{1,2}$ .

## VI. LEAKAGE AND FIDELITY OF THE TWO-QUBIT GATE

The intrinsic interqubit coupling in the SISIS gate is executed via weak Josephson supercurrents, the switching frequency of which is relatively low ( $\omega \sim 10^6 - 10^9 \text{ s}^{-1}$ ). The

supercurrents produce no noise in the junction;<sup>29</sup> thus, the coupling is “quiet.” Since there is no ac electric field in the SISIS junction, the disturbance of the surrounding circuit elements is negligible. Therefore, the current and charge noises are typically very low in the SISIS setup. However, the supercurrent is generated by an external circuit and the qubit will be exposed to noises of the circuit. Additionally, a dissipation in real SISIS gates is possible due to a tunneling of a quantum state through the characteristic barriers  $\Delta U_{1,2}(\phi)$  (see Fig. 4). Since the tunneling rate  $\Gamma$  depends on the barrier height and width exponentially, the populated upper level  $\varepsilon_2$  may in principle contribute to the dissipation, especially if one biases the system such that the tunneling rate  $\Gamma_2$  out of  $|2\rangle$  is  $\Gamma_2 \approx (\varepsilon_2 + \varepsilon_0 - 2\varepsilon_1)/2\pi$ . The relevant tunneling probability is  $P_t^{(2)} = \int p_2 \Gamma_2 dt$ . Although the  $P_t^{(2)}$  magnitude may be significant, the tunneling probabilities  $P_t^{(0)}$  and  $P_t^{(1)}$  out of states  $|0\rangle$  and  $|1\rangle$  are about  $10^3$  and  $10^6$  times lower as compared to  $P_t^{(2)}$ . The dissipation  $\mathcal{W}_2$  due to a transient population<sup>30</sup>  $p_2$  of state  $|2\rangle$  is estimated as  $\mathcal{W}_2 = \int \varepsilon_2 p_2 \Gamma_2 dt/\hbar$ . The last formula means that  $\mathcal{W}_2$  is roughly proportional to  $p_2$  and to the time of measurement,  $t_m$ . The dissipation is eliminated by keeping the population  $p_2$  of  $\varepsilon_2$  as small as possible and  $t_m$  as short as possible *during* the quantum logic operations.<sup>30</sup>

More essential in SISIS qubit gates is an intrinsic source of errors. Such errors come up when the interaction is turned on ( $J \neq 0$ ) and are caused by the *quantum leakage*. The leakage is taking place if the Hilbert space of the real gate is larger than the qubit’s computational subspace. A different time evolution in real space and in the computational subspace causes an error in the gate operation. An ideal unitary gate operation  $U_I(t)$  is obtained when turning on the interqubit coupling for a time  $t_0$ . By choosing  $t_0$  one may accomplish an arbitrary gate operation.<sup>1,11</sup> The output of an operation is related to the input state via the map  $\Pi U_R(t) \Pi$  where  $U_R(t)$  is the unitary operator which acts on the full Hilbert space and  $\Pi$  is the projector to the computational subspace acting as

$$\Pi \hat{H} \Pi = (|0\rangle\langle 0| + |1\rangle\langle 1|) \hat{H} (|0\rangle\langle 0| + |1\rangle\langle 1|), \quad (17)$$

where  $|0\rangle\langle 0| = (\hat{1} - \sigma_z)/2$ ,  $|1\rangle\langle 1| = (\hat{1} + \sigma_z)/2$ ,  $|0\rangle\langle 1| = (\sigma_x - i\sigma_y)/2$ , and  $|1\rangle\langle 0| = (\sigma_x + i\sigma_y)/2$ . The error of an operation is minimized by setting  $\Pi U_R(t) \Pi$  as close as possible to  $U_I(t_0)$ . In general an optimal operation requires  $t \neq t_0$  as all the system eigenvalues are modified by states outside the computational subspace. According to Refs. 25 and 26, the fidelity and leakage probabilities are defined as

$$F = 1 - \min_{\{t\}} \|U_I(t_0) - \Pi U_R(t) \Pi\|/2 \quad (18)$$

and

$$L(t) = 1 - \min_{\psi} \langle \psi | U_R^\dagger(t) \Pi U_R(t) | \psi \rangle. \quad (19)$$

The norm  $\|\cdot\|$  of an arbitrary operator  $K$  is defined as

$$\|K\| = \text{Sup}_{\psi} |K|\psi\rangle| = \text{Sup}_{\psi} \sqrt{\langle \psi | K^\dagger K | \psi \rangle} \quad (20)$$

over the vectors  $\{|\psi\rangle : \langle \psi | \psi \rangle = 1\}$  of the computational subspace. This definition implies that  $\|K\| = \sqrt{\kappa_M}$ , where  $\kappa_M$  is the largest eigenvalue of  $K^\dagger K$ . The evolution operator is

$$U_R(t) = \sum_n e^{-i\varepsilon_n t} |\Phi_n\rangle\langle \Phi_n| \quad (21)$$

(we set here  $\hbar = 1$ ). For a simple three-state analysis one uses that

$$|0\rangle = \begin{pmatrix} 1 \\ 0 \\ 0 \end{pmatrix}, \quad |1\rangle = \begin{pmatrix} 0 \\ 1 \\ 0 \end{pmatrix} \quad (22)$$

and that the eigenfunctions  $|\Phi_n\rangle$  of the Josephson energy potential of a noninteracting SIS junction at  $I_{1,2} = 0$  are expressed in terms of Mathieu functions. So the evolution in the computational subspace for a time interval  $t$  is

$$\begin{aligned} \Pi U_R(t) \Pi &= \sum_n e^{-i\varepsilon_n t} \Pi |\Phi_n\rangle\langle \Phi_n| \Pi = \sum_n e^{-i\varepsilon_n t} (|0\rangle\langle 0| + |1\rangle\langle 1|) \\ &\times |\Phi_n\rangle\langle \Phi_n| (|0\rangle\langle 0| + |1\rangle\langle 1|). \end{aligned} \quad (23)$$

The above equations (17)–(23) allow modeling of the basic two-qubit characteristics and simulation of the two qubit gate dynamics with qubit parameters computed in the former sections. According to Eq. (1), The basic parameters include the qubit energy level positions  $\varepsilon_{0,1,2}$ , the interlevel tunneling matrix element  $\tau$ , and the interqubit coupling energy  $J_{nm}$ . Major two-qubit gate characteristics, which are determined by the interqubit coupling and readout, are studied within the  $(3 \times 3)$ -state analysis. In that case one works with the six-dimensional Hilbert space of the real gate, which includes three states  $|0\rangle_n$ ,  $|1\rangle_n$ , and  $|2\rangle_n$  for each of the qubits  $n=1, 2$  affected by the interaction  $J$ . The computation is done in a straightforward way, using computer algebra and numeric methods. In this way one begins with microscopic computation of all the two-qubit parameters for given SISIS geometry, electrode purity, and temperature. The next stage involves a study of the interqubit interaction  $J$  and coupling to external meters. Finally one computes the major dissipative and dynamic properties of the two-qubit gates—i.e., the leakage and fidelity described by the Hamiltonian (1).

An illustrative insight into the two-qubit dynamics and dissipative characteristics is given by the analytical formulas derived in the former sections. Analytical solutions are available for a three-state single qubit gate and a  $(2 \times 2)$ -state two-qubit gate. One may, for instance, find an analytical expression for a resonant contribution to the leakage of a three-state system. The three-state system is described by the Hamiltonian

$$H^{3s} = \begin{pmatrix} -\varepsilon & \gamma & 0 \\ \delta & \varepsilon & \sqrt{2}\gamma \\ 0 & \sqrt{2}\delta & \varepsilon + \eta \end{pmatrix} \rightarrow \begin{pmatrix} E_0 & 0 & 0 \\ 0 & E_1 & 0 \\ 0 & 0 & E_2 \end{pmatrix}, \quad (24)$$

where the lowest level is positioned at  $-\varepsilon$ , and  $\delta$  and  $\gamma$  stand for the matrix elements of interlevel tunneling with the external field factors included. The arrow in Eq. (24) indicates

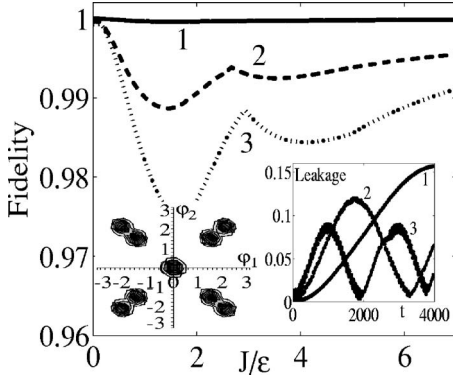


FIG. 6. Fidelity of the SISIS two-qubit gate for the levels  $\varepsilon_0^{(1,2)}=1$ ,  $\varepsilon_1^{(1,2)}=1$ , and  $\varepsilon_2^{(1,2)}=1.7$  and different tunneling matrix elements  $\tau=0.01, 0.6$ , and  $0.9$  for curves 1, 2, and 3, correspondingly. Dark spots in the left inset show regions of maximum entanglement. The right inset shows the related leakage probability curves versus time.

the diagonalization of  $H^{3s}$ . The eigenvectors of Eq. (24) are

$$|\Phi_0\rangle = \frac{1}{\sqrt{N}} \begin{pmatrix} \Theta_0 \\ \delta C_0 \\ \sqrt{2}\delta^2 \end{pmatrix}, \quad |\Phi_1\rangle = \frac{1}{\sqrt{N}} \begin{pmatrix} \Theta_1 \\ \delta C_1 \\ \sqrt{2}\delta^2 \end{pmatrix},$$

$$|\Phi_2\rangle = \frac{1}{\sqrt{N}} \begin{pmatrix} \Theta_2 \\ \delta C_2 \\ \sqrt{2}\delta^2 \end{pmatrix}, \quad (25)$$

where  $C_0 = P_- - 2(\varepsilon + \eta)/3$ ,  $C_{1,2} = C_{\pm} = (-P_- \mp i\sqrt{3}P_+)/2 - 2(\varepsilon + \eta)/3$ ,  $P_{\pm} = (B_0^2 \mp 4\varepsilon^2 + 2\varepsilon\eta + \eta^2)/(3B_0)$ ,  $B_0 = (3\varepsilon\eta^2 + \eta^3 + 3B_1 - 8\varepsilon^3 - 6\varepsilon^2\eta)^{1/3}$ , and  $B_1 = i(12\varepsilon^4\eta^2 + 3\varepsilon^2\eta^4 + 12\varepsilon^3\eta^3)^{1/2}$ . The above equations (24) and (25) allow a direct computation of the resonant contribution to the leakage at the frequency of external field  $\omega = (\varepsilon_1 - \varepsilon_0)/\hbar$ . As a result, one arrives at

$$\overline{L(t)}^4 = 1 - (\Theta_0^4 + \Theta_1^4 + \Theta_2^4 + \Theta_0^2\Theta_1^2 + \Xi^4)/N^4, \quad (26)$$

where  $\Xi^4 = |\gamma|\Theta_0\Theta_1(\Theta_0C_1 + \Theta_1C_0)$  and the normalizing factor is

$$N^4 = \Theta_0^4 + \Theta_1^4 + \Theta_2^4 + 2\Theta_0^2\Theta_1^2 + 2\Theta_1^2\Theta_2^2 + 2\Theta_0^2\Theta_2^2, \quad (27)$$

where  $\Theta_{0,1,2} = \Theta(E_{0,1,2})$  and the auxiliary function  $\Theta(\zeta)$  is

$$\Theta(\zeta) = (\zeta - \varepsilon)(\varepsilon - \zeta - \eta). \quad (28)$$

The eigenenergies of the Hamiltonian (24) are obtained as

$$E_0 = P_- + (\varepsilon + \eta)/3,$$

$$E_{1,2} = E_{\pm} = -P_-/2 + (\varepsilon + \eta)/3 \mp i\sqrt{3}P_+/2. \quad (29)$$

The corresponding analytical expression for the fidelity is much more cumbersome.

Typical calculation results of the fidelity and leakage probability versus time  $t$  are shown in Fig. 6. One can see that the fidelity of the SISIS gate shows anomalies when the interqubit coupling is sufficiently large—i.e., when it ex-

ceeds the splitting energy,  $J/\varepsilon > 1$ . If the coupling is small, the qubit gate fidelity is close to 1. The leakage probability versus the evolution time  $t$  oscillates with a large period which depends on the qubit parameters and the interqubit coupling, though it is small for  $t \leq 10^3$ . Optimal working regions are associated with an avoided-level crossing<sup>1,10</sup> where one achieves the maximum entanglement between the quantum states of the two SIS subjunctions. The entanglement is computed using Schmidt decomposition,<sup>31,32</sup> which represents any entangled state by a biorthogonal expression with positive real coefficients:

$$|\Psi(1,2)\rangle = \sum_{i=1} c_i |\alpha_i\rangle \otimes |\beta_i\rangle, \quad (30)$$

where  $|\alpha_i\rangle$  and  $|\beta_i\rangle$  are orthonormal states of subjunctions 1 and 2 and  $c_i$  are real and positive. The entanglement of a partially entangled pure state<sup>31,32</sup> is

$$\mathcal{E} = - \sum_i c_i^2 \log_2 c_i^2. \quad (31)$$

Since the interlevel spacing  $\varepsilon$ , tunneling amplitude  $\tau$ , and interqubit coupling  $J$  depend on the bias current  $I_b$ , the entanglement is computed self-consistently. Typical results for entanglement are shown in the contour plot (see the left inset in Fig. 6), where we assumed the junction transparency  $D = 10^{-4}$ ,  $d=3$ , and  $l_i/\xi=5$ . Dark spots in the  $\{\varphi_1, \varphi_2\}$  plane correspond to the avoided-level crossing (working) regions with the maximum inter-qubit entanglement.

The same QC coupling mechanism may be used for a controlled readout of the two-qubit state. Since the measurement is executed with weak supercurrents, there is no direct energy dissipation in the multibarrier Josephson junction. Instead dissipation occurs rather indirectly via tunneling through the characteristic barriers, as was mentioned at the beginning of this section. Quantum measurement of the qubit states<sup>33</sup> is furnished in a six-barrier multiterminal SISISIS-ISIS junction, where the two additional SISI subjunctions act as quantum meters. The SISI- and -ISIS sections measure the left- and right-side SIS subjunctions of the SISIS junction via the QC coupling. During the quantum measurement event the quantum states of SISI- and -ISIS sections are entangled with the adjacent SIS subjunction for a short time  $t_m \ll t_{dc}$  ( $t_{dc}$  is the decoherence time). To ensure a sufficient sensitivity of the measurement, one biases the measured SIS subjunction to get the upper level  $\varepsilon_2$  to be located at the top of the characteristic barrier  $\Delta U_{1,2}$ . The readout of the two-qubit states  $|\Phi_{1,2}\rangle$  is conducted by applying short pulses of ac supercurrent  $I_{1,2}^{ac}(t)$  to the SIS subjunctions. The  $\varepsilon_2$  level becomes populated with probability  $p_2(t)$ . The system then tunnels out from the populated state  $|2\rangle$  with the tunneling rate  $\Gamma_2$ . To evaluate the energy dissipation  $\mathcal{W}_2$ , we establish the time dependence of the upper-level population  $p_2(t)$ . This is done by introducing a fourth fictional auxiliary state  $|3\rangle_n$  (see, e.g., Ref. 30 and references therein). The tunneling from the state  $|2\rangle_{1,2}$  to the auxiliary state  $|3\rangle_n$  is described by the amplitude damping on fictitious qubits<sup>30</sup> within the  $(4 \times 4)$ -state analysis. The full space now includes four states for each of the qubits affected by the interaction  $J$ ,

which gives in total the eight-dimensional Hilbert space of the real two-qubit gate. Computation of the qubit characteristics and simulation of the qubit work both are conducted numerically. Initially one finds the parameters of the two-qubit Hamiltonian (1) as described in the former sections. Then the tunneling dynamics is modeled by using the operator-sum representation where an initial density matrix  $\hat{\rho}_i$  is mapped to the final density matrix  $\hat{\rho}_f$  as

$$\hat{\rho}_f = \sum_m \hat{E}_m \hat{\rho}_i \hat{E}_m^\dagger, \quad (32)$$

where  $\hat{E}_m$  are the Kraus operators.<sup>30</sup> The numeric analysis is performed by slicing the time dependence  $\hat{E}_m(t)$  in many discrete steps as described in Ref. 30. The input parameters include the junction parameters listed in Sec. IV, completed with the ac pulse amplitude and duration. We obtain the explicit form of the density matrix  $\hat{\rho}_i$  before the tunneling event. Then  $\hat{\rho}_i$  is mapped to  $\hat{\rho}_f$  in accordance with Eq. (32). Finally we determine the time dependence  $p_2(t)$ , which gives the dissipation  $\mathcal{W}_2$  for each of the meters and for given parameters of the six-barrier setup. In general, the dissipation introduced by a meter depends on the measurement time  $t_m$  and sensitivity of the meter. The sensitivity actually determines a minimal threshold magnitude of the energy dissipation  $\mathcal{W}_2$ , which must be sufficient for a firm readout. For a two-qubit gate with parameters used in Fig. 6 and  $J=0.2$  a most effective readout is achieved when  $\ln(t_{dc}/t_m) \simeq 10$  and  $I_0^{\text{ac}}/I_C \simeq 10^{-2}$  where  $t_{dc}$  is the decoherence time and  $I_0^{\text{ac}}$  is the

amplitude of the ac supercurrent pulse used to excite  $\varepsilon_2$  during the readout.

## VII. CONCLUSIONS

We conclude that the intrinsic coupling assures a low decoherence and dephasing of the two-qubit gate. If the measurement time  $t_m$  is sufficiently short while the tunneling current from the upper state through the characteristic barrier is small, the decoherence and dephasing are caused by the leakage only. The leakage comes from the induced changes in the Hilbert space of the real gate as considered above. This makes the intrinsic coupling mechanism attractive for use in two-qubit gates.

The suggested model quantitatively describes the general properties of the two-qubit gate with an externally controlled coupling. Since the coupling is intrinsic and coherent, it allows elimination of additional circuit elements and wirings. The QC coupling is tuned by the bias Josephson supercurrents which typically are much smaller than currents circulating in flux qubits. No charge accumulates on the coupling element in contrast to the case of two-qubit gates with a capacitive coupling. In this way noises and external sources of the decoherence in the system under study can be minimized. Nevertheless, one should pay attention to the remaining intrinsic sources of the decoherence, which persist during the two-qubit quantum logic operations.

## ACKNOWLEDGMENTS

This work was supported by the National Science Foundation under Grant No. EIA-0218652.

\*URL: <http://kyiv.phys.northwestern.edu>

<sup>1</sup>A. J. Berkley, H. Xu, R. C. Ramos, M. A. Gubrud, F. W. Strauch, P. R. Johnson, J. R. Anderson, A. J. Dragt, C. J. Lobb, and F. C. Wellstood, *Science* **300**, 1548 (2003).  
<sup>2</sup>Yu. A. Pashkin *et al.*, *Nature (London)* **421**, 823 (2003).  
<sup>3</sup>Y. Nakamura, Yu. A. Pashkin, and J. S. Tsai, *Nature (London)* **398**, 786 (1999).  
<sup>4</sup>D. Vion, A. Aassime, A. Cottet, P. Joyez, H. Pothier, C. Urbina, D. Esteve, and M. H. Devoret, *Science* **296**, 286 (2002).  
<sup>5</sup>J. R. Friedman *et al.*, *Nature (London)* **406**, 43 (2000).  
<sup>6</sup>C. H. van der Wal *et al.*, *Science* **290**, 773 (2000).  
<sup>7</sup>I. Chiorescu, Y. Nakamura, C. J. P. M. Harmans, and J. E. Mooij, *Science* **299**, 1869 (2003).  
<sup>8</sup>Y. Yu *et al.*, *Science* **296**, 889 (2002).  
<sup>9</sup>J. M. Martinis, S. Nam, J. Aumentado, and C. Urbina, *Phys. Rev. Lett.* **89**, 117901 (2002).  
<sup>10</sup>A. Blais, A. Maassen van den Brink, and A. M. Zagoskin, *Phys. Rev. Lett.* **90**, 127901 (2003).  
<sup>11</sup>R. C. Ramos, M. A. Gubrud, A. J. Berkley, J. R. Anderson, C. J. Lobb, and F. C. Wellstood, *IEEE Trans. Appl. Supercond.* **11**, 998 (2001); P. R. Johnson, F. W. Strauch, A. J. Dragt, R. C. Ramos, C. J. Lobb, J. R. Anderson, and F. C. Wellstood, *Phys. Rev. B* **67**, 020509(R) (2003); F. W. Strauch, P. R. Johnson, A. J. Dragt, C. J. Lobb, J. R. Anderson, and F. C. Wellstood, *Phys. Rev. Lett.* **91**, 167005 (2003).

<sup>12</sup>D. V. Averin and C. Bruder, *Phys. Rev. Lett.* **91**, 057003 (2003).  
<sup>13</sup>S. Russo, M. Kroug, T. M. Klapwijk, and A. F. Morpurgo, *Phys. Rev. Lett.* **95**, 027002 (2005).  
<sup>14</sup>S. E. Shafranjuk and J. B. Ketterson, *Phys. Rev. B* **72**, 212506 (2005).  
<sup>15</sup>G. Burkard, D. Loss, and E. V. Sukhorukov, *Phys. Rev. B* **61**, R16303 (2000).  
<sup>16</sup>Yu. Makhlin and G. Schön, *Rev. Mod. Phys.* **73**, 357 (2001).  
<sup>17</sup>G. A. Korn and T. M. Korn, *Mathematical Handbook for Scientists and Engineers* (McGraw-Hill, New York, 1968).  
<sup>18</sup>E. Prada and F. Sols, *Eur. Phys. J. B* **40**, 379 (2004).  
<sup>19</sup>I. P. Nevirkovets, O. Chernyashevskyy, and J. B. Ketterson, *IEEE Trans. Appl. Supercond.* **15**, 129 (2005); *J. Appl. Phys.* **97**, 123903 (2005).  
<sup>20</sup>I. P. Nevirkovets, S. E. Shafranjuk, and J. B. Ketterson, *Phys. Rev. B* **68**, 024514 (2003).  
<sup>21</sup>A. V. Svidzinsky, *Space-inhomogeneous Issues of the Superconducting Theory* (Science, Moscow, 1982) (in Russian).  
<sup>22</sup>A. V. Zaitsev, *Zh. Eksp. Teor. Fiz.* **86**, 1742 (1984) [*Sov. Phys. JETP* **59**, 1015 (1984)].  
<sup>23</sup>A. Shelankov and M. Ozana, *Phys. Rev. B* **61**, 7077 (2000).  
<sup>24</sup>S. E. Shafranjuk and J. B. Ketterson, *Phys. Rev. B* **72**, 024509 (2005).  
<sup>25</sup>R. Fazio, G. M. Palma, and J. Siewert, *Phys. Rev. Lett.* **83**, 5385 (1999); J. Siewert, R. Fazio, G. M. Palma, and E. Sciacca, J.

- Low Temp. Phys. **118**, 795 (2000); J. Siewert and R. Fazio, Phys. Rev. Lett. **87**, 257905 (2001).
- <sup>26</sup>F. Plastina, R. Fazio, and G. Massimo Palma, Phys. Rev. B **64**, 113306 (2001).
- <sup>27</sup>E. Merzbacher, *Quantum Mechanics* (Wiley, New York, 1998).
- <sup>28</sup>C. S. Owen and D. J. Scalapino, Phys. Rev. **164**, 538 (1967).
- <sup>29</sup>K. K. Likharev, *Dynamics of Josephson Junctions and Circuits* (Gordon and Breach, New York, 1986).
- <sup>30</sup>M. Steffen, J. M. Martinis, and I. L. Chuang, Phys. Rev. B **68**, 224518 (2003).
- <sup>31</sup>A. Peres, *Quantum Theory: Concepts and Methods* (Kluwer, Dordrecht, 1993).
- <sup>32</sup>C. H. Bennett, H. J. Bernstein, S. Popescu, and B. Schumacher, Phys. Rev. A **53**, 2046 (1996).
- <sup>33</sup>I. Siddiqi, R. Vijay, F. Pierre, C. M. Wilson, M. Metcalfe, C. Rigetti, L. Frunzio, and M. H. Devoret, Phys. Rev. Lett. **93**, 207002 (2004).